Single-molecule tracking in live *Yersinia enterocolitica* reveals distinct cytosolic complexes of injectisome subunits

*Julian Rocha[a], Charles Richardson[a], Mingxing Zhang[a], Caroline Darch[a], Eugene Cai[a], Andreas Diepold[b], Andreas Gahlmann[a,c,]**

[a]Department of Chemistry, University of Virginia, Charlottesville, VA 22904

[b]Max Planck Institute for Terrestrial Microbiology, Karl-von-Frisch-Strasse 10, 35043 Marburg, Germany

[c]Department of Molecular Physiology & Biological Physics, University of Virginia School of Medicine, Charlottesville, VA 22904

Keywords: type 3 secretion, injectisome, sorting platform, super-resolution, fluorescence, live-cell, single-molecule, tracking.

Abstract

In bacterial type 3 secretion, substrate proteins are actively transported from the bacterial cytoplasm into the cytoplasm of host cells by a large membrane-embedded machinery called the injectisome. Injectisomes transport secretion substrates in response to specific environmental signals, but the molecular details by which the cytosolic secretion substrates are selected and transported through the type 3 secretion pathway remain unclear. Secretion activity and substrate selectivity are thought to be controlled by a sorting platform consisting of the proteins SctK, SctQ, and SctL, which together localize to the cytoplasmic side of membrane-embedded injectisomes. However, recent work revealed that sorting platform proteins additionally exhibit substantial cytosolic populations and that SctQ reversibly binds to and dissociates from the cytoplasmic side of membrane-embedded injectisomes. Based on these observations, we hypothesized that dynamic molecular turnover at the injectisome and cytosolic assembly among sorting platform proteins is a critical regulatory component of type 3 secretion. To determine whether intact sorting platform complexes exist in the cytosol of living cells, we measured the diffusive properties of thousands of SctQ and SctL proteins using high-throughput 3D single-molecule tracking microscopy. The obtained single-molecule trajectories reveal that both SctQ and SctL exist in several distinct diffusive states in the cytosol of living *Yersinia enterocolitica*, indicating that these proteins are able to form stable oligomeric complexes in their native environment. Our findings provide new insights into the dynamic regulatory network that interfaces stationary membrane-embedded injectisomes with the soluble cytosolic components of the T3SS.

Significance Statement

Type 3 secretion system (T3SS) injectisomes are used for inter-kingdom transfer of proteins between bacterial pathogens and eukaryotic cells. In spite of recent progress in determining the *in situ* morphology of fully assembled injectisomes, the functional regulation of the T3SS remains unresolved. Using 3D single-molecule tracking microscopy, we found that injectisome subunits that are thought to control the substrate selectivity of the T3SS assemble into high molecular weight complexes in the cytosol of living cells. The formation of these complexes requires the presence of other T3SS proteins and correlates with the cell's secretion activity. Cytosolic assembly of protein subunits may be a general mechanism to control the T3SS and similar membrane-embedded biomolecular assemblies.

Introduction

Bacteria can secrete intact macromolecules into the surrounding medium or into nearby cells through broadly-conserved large biomolecular assemblies, called secretion systems (1). Type 3 secretion systems (T3SSs) are used by bacteria for flagellar biogenesis and for virulence (2). The virulence-associated T3SS, also called the injectisome, features a long hollow needle that protrudes perpendicularly from the bacterial cell surface and ultimately anchors itself into the host cell membrane (**Fig. 1**) (2-5). T3SS injectisomes target host cell biology through the translocation of species-specific effector proteins into the cytoplasm of the host cells. The structural proteins of the T3SS injectisome are highly conserved among prominent Gram-negative pathogens, including *Salmonella*, *Shigella*, *Yersinia*, *Pseudomonas*, and *E. coli*, making T3SSs broadly utilized protein delivery machines (4).

A still incompletely understood feature of virulent T3SSs is that secretion can be activated in response to environmental cues and that secretion substrate selectivity follows a well-defined temporal hierarchy (6). Expression and assembly of the injectisome is triggered by a temperature jump to 37°C experienced upon entry into mammalian hosts (3). Early substrates of the secretion-competent injectisome are proteins that assemble the needle itself. Once the needle has reached a certain length, selectivity is switched to middle secretion substrates that form the translocon pore, which anchors the needle tip into the host cell membrane. Finally, selectivity switches again upon stable injectisome-mediated host cell contact (7) or in response to external cues, such as calcium chelation in *Yersinia* (8), to allow secretion of late secretion substrates, namely the effector proteins (5). The recognition and selection of export substrates is hypothesized to result from coordinated interactions among the cytoplasmic components of the injectisome, which attach to the membrane-embedded rings of the injectisomes (**Fig. 1**) (9-11).

In vitro genetic and proteomic experiments in *Yersinia* and other pathogens have identified several cytoplasmic injectisome subunits whose direct interactions with each other are essential for type 3 secretion (12-16). In particular, the proteins SctK, SctQ, SctL, and SctN (YscK, YscQ, YscL, and YscN in *Yersinia*; the universal nomenclature is used throughout this manuscript) have been found to form sorting platforms, which are high molecular weight complexes that interact both with needle complexes *and* sequentially with different secretion substrates and their cognate cytosolic chaperones (16, 17). The *sctQ* gene in *Y. enterocolitica* additionally contains an internal translation initiation site, and thus produces two separate gene products: the full-length protein ($SctQ_{FL}$) that contains all 307 amino acid residues and the C-terminal fragment ($SctQ_C$) that contains amino acid residues 218−307 (18, 19). All of these proteins localize together at membrane-embedded injectisomes, which is essential for secretion (20, 21).

The precise positions of the sorting platform proteins SctK, SctQ, SctL, and the ATPase SctN within the *in situ* quaternary structure of fully assembled injectisomes have recently been determined by cryo-electron tomography (9-11). The 3D tomogram averages reveal a cytoplasmic injectisome complex of hexametric symmetry, which is notably different from the continuous cytoplasmic ring (C-ring) structure observed in flagellar T3SSs (22-24). The cytoplasmic complex of the injectisome consists of six SctQ, and likely $SctQ_C$, containing "pods" that attach to the membrane-embedded ring of the needle complex, presumably through SctK (10). Each pod further connects to one of six spokes of a cradle-like structure formed by SctL that holds in place the central hexameric SctN (**Fig. 1**). The morphology of *in situ* injectisomes provides an important structural foundation for any proposed type 3 secretion

mechanism. However, deciphering the dynamic functional regulation of T3SSs requires live-cell compatible approaches.

Live-cell measurements in *Y. enterocolitica* using fluorescence recovery after photobleaching (FRAP) established that the sorting platform protein SctQ continuously exchanges between an injectisome bound state and a freely diffusing cytosolic state (20). Exchange of eGFP-SctQ subunits was accelerated in *Yersinia* injectisomes when effector protein secretion was chemically induced by calcium chelation. Other sorting platform proteins, SctK, SctL, and SctN, also exhibit significant cytosolic populations (16, 17, 21). Fluorescence correlation spectroscopy (FCS) measurements revealed that the mean diffusion coefficients of these sorting platform components varied between different deletion mutants, indicating that these proteins interact with each other and likely form hetero-oligomeric molecular complexes in the cytosol (21). These observations led to the hypothesis that dynamic molecular turnover at the injectisome and cytosolic assembly among sorting platform proteins is an important regulatory component of type 3 secretion. Gaining further insights into the underlying regulatory network requires resolving the cytosolic diffusion properties of individual T3SS proteins and their molecular complexes in living cells.

Here we report high-throughput 3D single-molecule tracking measurements to determine the diffusive behaviors of thousands of individual SctQ and SctL fusion proteins in living *Y. enterocolitica*. Our results demonstrate that the two central sorting platform proteins, SctQ and SctL, interact with each other and with other T3SS proteins not just at the injectisome, but also in the cytosol of living cells. By modelling the effects of anisotropic molecular confinement inside rod-shaped bacterial cells, we found that both SctQ and SctL exist in different cytosolic diffusive states. Determining the unconfined diffusion coefficient and relative population fraction of each

diffusive state allowed us to compare the diffusion properties of SctQ and SctL under secreting and non-secreting conditions and in different genetic backgrounds. The combined results are consistent with a model in which SctQ and SctL co-diffuse as part of a large cytosolic complex that forms only in the presence of other T3SS proteins. Defining how the T3SS relies on the hierarchical assembly of its components in the cytosol of living cells will help identify key vulnerabilities that may be exploited to control the bacterial virulence mechanisms that depend on type 3 secretion.

Results/Discussion

Stationary SctQ localizes near the cell membrane. We introduced the coding sequence of eYFP in-frame near the translation start site of the SctQ coding sequence on the pYV virulence plasmid, which encodes all T3SS proteins in *Y. enterocolitica*, using previously described allelic replacement techniques (25, 26). In this way, the eYFP-SctQ fusion protein is expressed under the control of its native promoter. We confirmed that the resulting fusion proteins did not result in detectable degradation products and were fully functional in an effector protein secretion assay (**Fig. S1**). We then used 3D-single molecule localization microscopy (3D-SMLM) to determine the subcellular positions of eYFP-SctQ molecules in live *Y. enterocolitica* under secreting conditions. The observed single-molecule localizations exhibited clustering near the cell surface, and, when rendered as an intensity image, these clusters gave rise to the bright fluorescent foci (**Fig. 2 A and B**), which are similar to diffraction-limited epifluorescence microscopy observations (26). We used DBSCAN (27), a density-based clustering algorithm, to determine the positions and sizes of each cluster and found that clusters are preferentially localized within a 400-450 nm radius from the central cell axis (**Fig. 2C**). This subcellular preference is consistent with membrane association, given the 469 ± 91 nm (mean ± s.d.) radius of *Y. enterocolitica* cells used in our experiments, and clusters have been previously observed to co-localize with other membrane-embedded injectisome components in two-color fluorescence imaging experiments (20, 26, 28). In contrast, cluster formation was not observed when we exogenously expressed eYFP-SctQ in a *Y. enterocolitica* strain lacking the pYV plasmid (pYV-) (**Fig. 2D**). Instead, eYFP-SctQ was uniformly distributed throughout the bacterial cytosol.

Single-molecule tracking measurements in wild-type cells showed that the eYFP-SctQ population partitioned into a stationary and a mobile fraction (**Fig. 2E**). Trajectories with slow

apparent diffusion coefficients ($D^* < 0.15$ μm^2/s) spatially co-localize with clusters (**Fig. 2F and Fig. S7A**), while the faster diffusing molecules ($D^* > 0.15$ μm^2/s) localize randomly throughout the cell volume (**Fig. 2E inset, Fig. S7A)**. This apparent diffusion coefficient threshold was chosen based on the non-zero diffusion coefficients obtained for stationary emitters that are repeatedly localized with limited localization precision (**Fig. S5**). We conclude that stationary membrane-embedded injectisomes serve as binding sites for SctQ molecules, and we assign the observed clusters or foci to injectisome-bound eYFP-SctQ molecules.

SctQ exists in at least 3 diffusive states in the bacterial cytosol. The majority (~86%) of eYFP-SctQ localizations are not cluster-associated, but instead diffuse randomly throughout the cytoplasm (**Fig. 2 A, B, and C**). To examine the diffusive behaviors of unbound eYFP-SctQ, we determined the 3D trajectories of ~100,000 individual eYFP-SctQ molecules in hundreds of cells and computed the apparent diffusion coefficients for each trajectory (**Supplementary Information**). As mentioned in the previous section, the resulting distribution of apparent diffusion coefficients shows two prominent peaks: one near ~0 μm^2/s and the other at ~0.5 μm^2/s (**Fig. 2E**). In addition to the peak at ~0.5 μm^2/s, the distribution also shows a slow decay towards higher apparent diffusion coefficients. Using Monte Carlo simulations of anisotropically confined Brownian diffusion within rod-shaped bacterial cell volumes, we determined that such a distribution shape is only possible when multiple diffusive states are manifested in the cell (**Supplemental Information, Fig. S2**).

To estimate the unconfined diffusion coefficients (D) and population fractions of the diffusive states represented in the confined apparent diffusion coefficient (D^*) distribution, we used linear combinations of simulated apparent diffusion coefficient distributions to fit the

experimental empirical cumulative distribution function (eCDF) (**Supplementary Information**). Using the eCDF instead of a probability density function (PDF) histogram eliminates bin-size ambiguities that can bias the fitting results. We found that fitting the eYFP-SctQ eCDF required three cytosolic diffusive states corresponding to unconfined diffusion coefficients D = 1.1, 4.0, and 13.9 $\mu m^2/s$ with population fractions of 17%, 36%, and 22%, respectively (**Fig. 3 A and B, Table 1**). These components are in addition to a stationary component ($D < 0.5\ \mu m^2/s$) with population fraction of 24%. Confidence intervals for the optimized fitting parameters were obtained by bootstrapping and are reported in **Table S2**.

As we did not detect any eYFP cleavage products (**Fig. S1**), the eYFP-SctQ monomer is the smallest and likely the fastest diffusing molecular species in our cells. Control experiments to measure the unconfined diffusion coefficients of eYFP confirmed that, when expressed in wild-type *Y. enterocolitica*, eYFP diffused at similarly fast rates, D = 9.5 and 13.5 $\mu m^2/s$, which likely represents the propensity of eYFP to dimerize and oligomerize (29, 30) (**Fig. S4H, Table 1**). We also observe a small stationary component for this protein suggesting that, even in the absence of known binding partners, the presence of immobile proteins cannot be ruled out in living cells. Assigning the fastest diffusive eYFP-SctQ state (D = 13.9 $\mu m^2/s$) to the monomeric eYFP-SctQ fusion protein implies that the slower diffusive states at $D \sim 1$ and 4 $\mu m^2/s$ correspond to two distinct high molecular weight complexes, which could be eYFP-SctQ homo- or hetero-oligomers that involve additional T3SS proteins. To elucidate the molecular composition of these high molecular weight complexes, we performed further single-molecule tracking measurements in different genetic backgrounds.

SctQ is capable of forming higher-order oligomers in the absence of other T3SS proteins. To test whether SctQ can form high molecular weight complexes in living cells independent of other T3SS proteins, we tracked single eYFP-SctQ molecules in a strain lacking all T3SS components (the pYV- strain), for which membrane association was not observed (**Fig. 2D**). Fitting the distribution of apparent diffusion coefficients of eYFP-SctQ in the pYV- strain required four diffusive states (**Fig. 4A, Table 1**). The predominant diffusive state (D = 3.6 μm^2/s, 78%) is similar to the D = 4.0 μm^2/s state observed for eYFP-SctQ in wild-type cells. These data show that formation of a specific oligomeric SctQ species is favored in pYV- cells and does not require any other T3SS proteins. Conversely, the oligomerization behavior of eYFP-SctQ changes when other T3SS proteins are present, as there is a higher relative abundance of the putative eYFP-SctQ monomer in wild-type cells (22%) compared to pYV- cells (~5%). If oligomerization of SctQ was completely unregulated we would expect a higher fraction of the $D \sim 4$ μm^2/s diffusive state in wild-type cells, especially since eYFP-SctQ is slightly overexpressed compared to the native, unlabeled protein (**Fig. S1**).

Formation of the oligomeric SctQ complex is dependent on expression of SctQ$_C$. Previous work in *Yersinia* has shown that elimination of the internal translation initiation site through a mutation in the *sctQ* coding sequence that replaces the methionine residue at position 218 with an alanine (M218A) results in a secretion-deficient phenotype and that wild-type secretion levels can be restored upon expression of SctQ$_C$ *in trans* (19, 20). We therefore hypothesized that the $D \sim 4$ μm^2/s diffusive state measured for eYFP-SctQ in wild-type cells and pYV- background is due to a molecular complex containing SctQ and its C-terminal fragment

$SctQ_C$ (18, 19, 31). To test this hypothesis, we utilized the *eyfp-sctQ$_{M218A}$* coding sequence to express full length eYFP-SctQ, but not $SctQ_C$, in the *Y. enterocolitica* pYV- strain (20).

In the absence of $SctQ_C$, the distribution of apparent diffusion coefficients of eYFP-$SctQ_{M218A}$ was fit with four diffusive states (**Fig. 4B, Table 1**). The previously observed diffusive state ($D \sim 4$ μm^2/s) of eYFP-SctQ is absent upon elimination of $SctQ_C$ expression. We instead observe a different, faster moving diffusive state ($D = 6.8$ μm^2/s), which is not observed for eYFP-SctQ in either wild-type or pYV- genetic backgrounds. We therefore assign the $D = 6.8$ μm^2/s diffusive state to a homo-oligomeric SctQ species. Indeed, an oligomeric SctQ-only species was previously detected by co-immunoprecipitation in the absence of $SctQ_C$ (18). We conclude that the presence of $SctQ_C$ enables the formation of a well-defined oligomeric SctQ:$SctQ_C$ complex, which diffuses at $D \sim 4$ μm^2/s and forms spontaneously in *Y. enterocolitica* in the absence of other T3SS proteins.

The existence of an oligomeric SctQ:$SctQ_C$ complex is supported by several reports in the recent literature. Bzymek *et al.* expressed *Y. pseudotuberculosis* SctQ and $SctQ_C$ in *E. coli* and co-purified a SctQ:$SctQ_C$ complex with 1:2 stoichiometry (*MW* = 52.8 kDa) (19). McDowell *et al.* found that *S. flexneri* SctQ:$SctQ_C$ was further able to form higher order oligomers consisting of up to six copies of the minimal 1:2 complex and that formation of such higher order oligomers was essential for secretion (31). The quaternary structure of *in situ* injectisomes, recently provided by cryo-electron tomography of *Shigella flexneri* and *Salmonella enterica* minicells (9-11), allows us to further speculate on the stoichiometry of the oligomeric SctQ:$SctQ_C$ complex. The sub-tomogram averaged injectisomes displayed six cytoplasmic "pods" that, on one side, attach to the membrane-embedded ring of the needle complex and, on the other side, to hexameric SctN. The observed protein densities of the pods are large enough to

contain a tetramer of SctQ proteins, such that 24 SctQ molecules (six tetramers) can be bound to the injectisome at any one time. This value agrees with previously estimated numbers of fluorescently-labelled SctQ proteins within a single diffraction-limited fluorescent focus/cluster (N = 22 ± 8, ~24 ± 5, 28 ± 7) (20, 21, 28). Based on the available data to date, we speculate that the $D \sim 4$ μm^2/s diffusive state observed in wild-type *Y. enterocolitica* cells is the oligomeric SctQ:SctQ$_C$ complex that consists of four SctQ and eight SctQ$_C$ subunits.

SctQ and SctL co-diffuse as a complex in the cytoplasm. Our single-molecule tracking measurements of eYFP-SctQ in wild-type *Y. enterocolitica* reveal the presence of a slowly diffusing $D \sim 1$ μm^2/s species with a population fraction of 17%. The increased abundance of this diffusive state compared to pYV- cells could indicate the regulated formation of a slowly diffusing high-molecular weight complex. Indeed, high molecular weight complexes with estimated molecular weights ~1 MDa containing SctQ, SctL, SctK, and SctN have been previously identified in pull-downs and size-exclusion chromatography (16, 17). Given the established interactions between the soluble T3SS components SctK-Q-L-N (12-15), we hypothesized that the $D \sim 1$ μm^2/s diffusive state consists, at least partially, of a complex containing not just SctQ:SctQ$_C$, but also SctK, SctL, and possibly SctN (see **Fig. 1**).

To test whether the $D \sim 1$ μm^2/s or $D \sim 4$ μm^2/s diffusive states of eYFP-SctQ are complexes that contain SctL, we used allelic-replacement of the native SctL coding sequence on the pYV virulence plasmid to express the PAmCherry1-SctL fusion protein in wild-type *Y. enterocolitica*. Fitting the apparent diffusion coefficient distribution of PAmCherry1-SctL revealed a substantial stationary population ($D < 0.50$ μm^2/s) with a population fraction of 56%. Stationary PAmCherry1-SctL trajectories ($D^* < 0.15$ μm^2/s) localized preferentially near the cell

boundary (**Fig. S7E**). Based on the same arguments made for eYFP-SctQ, we assign the stationary PAmCherry1-SctL trajectories to injectisome-bound molecules. Fitting the non-stationary components of the apparent diffusion coefficient distribution revealed the presence of five diffusive states (**Fig. 5A, Table 1**). The only observed diffusive states in common between eYFP-SctQ and PAmCherry1-SctL in wild-type *Y. enterocolitica* is the $D \sim 1$ μm^2/s state. The presence of this common state raises the possibility that these two proteins co-diffuse as a high-molecular weight complex in the cytosol of living cells.

To test whether the $D \sim 1$ μm^2/s diffusive state of PAmCherry1-SctL is dependent on the presence of SctQ and other T3SS proteins, we expressed PAmCherry1-SctL in the pYV- strain. In this genetic background, the apparent diffusion coefficient distribution is fit by four diffusive states (**Fig. 5B, Table 1**). A majority of the stationary component is lost in the absence of other T3SS proteins and the population fractions are redistributed to other cytosolic states. Notably absent is a diffusive state near 1 μm^2/s, indicating that the presence of other T3SS proteins is required for the formation of this state.

A high molecular weight complex containing SctQ, SctQ$_C$, SctK, SctL, and SctN is consistent with previous FCS measurements showing that the average diffusion rate of eGFP-SctQ and eGFP-SctL increased when SctN was deleted (21). It is therefore possible that the $D \sim 1$ μm^2/s diffusive state observed in our work is due to the cytosolic presence of a large supramolecular complex that contains six SctK-Q-L pods, which are each connected to a central hexameric ATPase. Such a supramolecular complex would have a molecular weight of ~2 MDa, assuming previously estimated stoichiometries (9, 10, 20, 21, 28), and could form either through the stepwise assembly in the cytoplasm or upon concerted dissociation from membrane-embedded injectisomes. An alternative explanation is that the $D \sim 1$ μm^2/s diffusive state

represents a single pod that is connected to SctL and possibly SctK and SctN. Even though the Stokes-Einstein relation is not expected to hold in the crowded cytoplasm of living bacterial cells (32, 33), it is not clear how the rather modest addition of SctL (2x25 kDa), SctK (24 kDa), and SctN (48 kDa) subunits to an existing $SctQ_4$:$SctQ_{C8}$ complex (330 or 220 kDa with and without the eYFP tag, respectively) could change its diffusion coefficient by a factor of four. Future work to determine the complete molecular composition of the $D \sim 1$ μm^2/s diffusive state will help address this question.

Induction of T3SS secretion alters diffusion behaviors of select cytosolic species. FRAP measurements established that, under secreting conditions, injectisome-bound eGFP-SctQ was dynamically replaced by new cytosolic proteins within $t_{½} \sim 70$ seconds ($t_{½} \sim 135$ seconds in non-secreting *Y. enterocolitica* cells) (20). Additionally, previous FCS measurements found that the average diffusion rates of SctK, SctQ, and SctL correlate with the secretion state (21). Our results show that the T3SS proteins SctQ and SctL form high molecular weight complexes in the cytosol and that formation of these states is dependent on the presence of other T3SS proteins. Together, these findings suggest the possibility that the type 3 protein secretion pathway is, at least partially, regulated from within the cytosol. We therefore asked whether the diffusion rates or population fractions of SctQ and SctL diffusive states correlate with the secretion state of the cells.

To compare the diffusion behaviors of eYFP-SctQ and PAmCherry1-SctL in secretion ON vs. OFF states we used the fact that the *Y. enterocolitica* T3SS can be switched between secretion ON and OFF states by the addition of EDTA or $CaCl_2$, respectively (8). For both eYFP-SctQ and PAmCherry1-SctL, we observed an overall slowing of diffusion rates when cells

were in the secretion OFF state, consistent with recent FCS and earlier 2D-PALM measurements (20, 21). Stimulation of secretion increased the mean apparent diffusion coefficient for mobile molecules ($D^* > 0.15$ μm^2/s) from 1.43 μm^2/s to 1.69 μm^2/s for eYFP-SctQ and from 0.86 μm^2/s to 1.10 μm^2/s for PAmCherry1-SctL (**Table S3)**.

The apparent diffusion coefficient distribution of eYFP-SctQ in secretion OFF conditions was fit with three diffusive states (**Fig. 6A, Table 1**), while that of PAmCherry1-SctL was fit with four diffusive states (**Fig. 6B, Table 1**). The diffusion coefficients obtained for eYFP-SctQ are similar between secretion ON and OFF conditions, suggesting that oligomeric states of SctQ are not altered upon induction of secretion. However, the relative population fractions do change, suggesting that the relative abundances of SctQ containing complexes are regulated. For PAmCherry1-SctL on the other hand, there seems to be a more complex rearrangement among diffusive states of low abundance. Nonetheless, the presence of the D ~ 1 μm^2/s diffusive state for both eYFP-SctQ and PAmCherry1-SctL under secretion ON and secretion OFF conditions indicates that the cytosolic interaction between SctQ and SctL is robustly present in both secreting and non-secreting cells. Furthermore, we observe a similar decrease in the relative population fractions of the $D \sim 1$ μm^2/s diffusive states upon induction of secretion, namely a 26% decrease for eYFP-SctQ and a 24% decrease for PAmCherry1-SctL. These results support our conclusion that SctQ and SctL co-diffuse as high molecular weight complex in the cytosol and suggest that the strength of the SctQ and SctL interaction is not subject to functional regulation of the T3SS ON/OFF switch.

Conclusions

Using live-cell high-throughput 3D single-molecule tracking combined with a quantitative analysis framework based on Monte Carlo simulations of anisotropically confined

Brownian motion, we resolved the diffusive states of eYFP-SctQ and PAmCherry1-SctL and quantified their respective population fractions within living bacterial cells. Our data are consistent with a model in which cytosolic SctQ undergoes dynamic assembly and disassembly steps to interconvert between at least three distinct molecular species that diffuse at different rates. SctQ monomers diffuse freely in the cytosol ($D \sim 14$ μm^2/s) or self-assemble into oligomeric SctQ:SctQ$_C$ complexes ($D \sim 4$ μm^2/s) with the help of the C-terminal fragment SctQ$_C$. The self-assembly process does not require the presence of other T3SS proteins as evidenced by the observation that a $D \sim 4$ μm^2/s diffusive state is present in both wild-type and pYV- backgrounds. The SctQ:SctQ$_C$ complexes do not yet contain SctL, because SctL molecules tracked in wild-type cells do not exhibit a $D \sim 4$ μm^2/s diffusive state. However, it remains a possibility that SctQ;SctQ$_C$ complexes in wild-type cells contain SctK, which has been shown to interact with SctQ (12-15). Ultimately, the SctQ;SctQ$_C$ complexes further associate with SctL, SctK, and possibly SctN to form hetero-oligomeric high molecular weight complexes that give rise to the $D \sim 1$ μm^2/s diffusive state. The presence of a $D \sim 1$ μm^2/s diffusive state in both the eYFP-SctQ and PAmCherry1-SctL data suggest that SctQ and SctL co-diffuse as part of high molecular weight complexes, but it remains to be determined whether these complexes are individual sorting platform pods or large supramolecular complexes containing six pods that are each connected to a central hexameric ATPase.

Our work adds to a growing body of evidence that points to the existence of a dynamic network of cytosolic interactions among structural injectisome proteins and complexes thereof. The observations that either the relative abundances of diffusive states (for SctQ) or the diffusive states themselves (for SctL) are altered upon induction of secretion suggest a delocalized mechanism of T3SS functional regulation: The activity and substrate selectivity of T3SSs is not

programmed into the quaternary structure of the injectisome itself, but instead established in the cytosol through dynamic interactions between T3SS components. Given the *in situ* morphology of injectisomes, it is tempting to speculate that molecular turnover at the injectisome is the result of dynamic binding and unbinding events of intact sorting platform pods and/or entire injectisome cytoplasmic complexes. Such dynamics may help regulate the secretion activity of the T3SS or enable the shuttling of secretion substrate:chaperone complexes to the injectisome. High-throughput single-molecule tracking in different genetic backgrounds will help distinguish between these possibilities by determining which molecular interactions are necessary and sufficient for the formation of specific cytosolic complexes in living cells.

Materials and Methods

All *Y. enterocolitica* strains are listed in **Table S1**. Experiments and data analysis methods are describe in detail in the Supplemental Information. 3D super-resolution imaging was performed with a custom-built imaging system. Image analysis was performed using a modified version of the easy-DHPSF software (34). Cluster analysis was performed using the DBSCAN clustering algorithm (27). Apparent diffusion coefficients were obtained by linking 3D single-molecule localizations in the same cell in subsequent frames. Unconfined diffusion coefficient values were obtained using a quantitative analysis framework based on Monte Carlo simulations of anisotropically confined Brownian diffusion within rod-shaped bacterial cell volumes.

Acknowledgments

We thank Linda Columbus and Jim Casanova for critical reading of the manuscript. This work was supported by the startup funds from the University of Virginia (to A.G.). We also thank Judith P. Armitage for stimulating discussions.

Author contributions:

J.R., C.R., A.D., and A.G. and designed research;

J.R. and A.D. performed research;

J.R., C.R., M.Z., C.D., E.C., A.D., and A.G. contributed new reagents/analytic tools;

J.R., C.R., and A.G. analyzed data;

and J.R., C.R. A.D., and A.G. wrote the paper.

References

1. Costa TR, *et al.* (2015) Secretion systems in Gram-negative bacteria: structural and mechanistic insights. *Nature reviews. Microbiology* 13(6):343-359.
2. Diepold A & Armitage JP (2015) Type III secretion systems: the bacterial flagellum and the injectisome. *Philosophical transactions of the Royal Society of London. Series B, Biological sciences* 370(1679).
3. Cornelis GR (2006) The type III secretion injectisome. *Nature reviews. Microbiology* 4(11):811-825.
4. Buttner D (2012) Protein export according to schedule: architecture, assembly, and regulation of type III secretion systems from plant- and animal-pathogenic bacteria. *Microbiology and molecular biology reviews : MMBR* 76(2):262-310.
5. Portaliou AG, Tsolis KC, Loos MS, Zorzini V, & Economou A (2016) Type III Secretion: Building and Operating a Remarkable Nanomachine. *Trends Biochem Sci* 41(2):175-189.
6. Deng W, *et al.* (2017) Assembly, structure, function and regulation of type III secretion systems. *Nature reviews. Microbiology*.
7. Martinez-Argudo I & Blocker AJ (2010) The Shigella T3SS needle transmits a signal for MxiC release, which controls secretion of effectors. *Molecular microbiology* 78(6):1365-1378.
8. Lee VT, Mazmanian SK, & Schneewind O (2001) A program of Yersinia enterocolitica type III secretion reactions is activated by specific signals. *Journal of bacteriology* 183(17):4970-4978.
9. Liu J, Kumar P, Hu Y, Cheng GJ, & Irudayaraj J (2015) Enhanced Multiphoton Emission from CdTe/ZnS Quantum Dots Decorated on Single-Layer Graphene. *The Journal of Physical Chemistry C* 119(11):6331-6336.
10. Hu B, Lara-Tejero M, Kong Q, Galán JE, & Liu J (2017) In Situ Molecular Architecture of the Salmonella Type III Secretion Machine. *Cell* 168(6):1065-1074.e1010.
11. Makino F, *et al.* (2016) The Architecture of the Cytoplasmic Region of Type III Secretion Systems. *Scientific Reports* 6:33341.
12. Jackson MW & Plano GV (2000) Interactions between type III secretion apparatus components from Yersinia pestis detected using the yeast two-hybrid system. *FEMS Microbiology Letters* 186(1):85-90.
13. Jouihri N, *et al.* (2004) MxiK and MxiN interact with the Spa47 ATPase and are required for transit of the needle components MxiH and MxiI, but not of Ipa proteins, through the type III secretion apparatus of Shigella flexneri. *Molecular microbiology* 49(3):755-767.
14. Morita-Ishihara T, *et al.* (2006) Shigella Spa33 is an essential C-ring component of type III secretion machinery. *The Journal of biological chemistry* 281(1):599-607.
15. Spaeth KE, Chen YS, & Valdivia RH (2009) The Chlamydia type III secretion system C-ring engages a chaperone-effector protein complex. *PLoS Pathog* 5(9):e1000579.
16. Johnson S & Blocker A (2008) Characterization of soluble complexes of the Shigella flexneri type III secretion system ATPase. *FEMS Microbiol Lett* 286(2):274-278.
17. Lara-Tejero M, Kato J, Wagner S, Liu X, & Galan JE (2011) A Sorting Platform Determines the Order of Protein Secretion in Bacterial Type III Systems. *Science* 331(6021):1188-1191.

18. Yu XJ, Liu M, Matthews S, & Holden DW (2011) Tandem translation generates a chaperone for the Salmonella type III secretion system protein SsaQ. *The Journal of biological chemistry* 286(41):36098-36107.
19. Bzymek KP, Hamaoka BY, & Ghosh P (2012) Two translation products of Yersinia yscQ assemble to form a complex essential to type III secretion. *Biochemistry* 51(8):1669-1677.
20. Diepold A, Kudryashev M, Delalez NJ, Berry RM, & Armitage JP (2015) Composition, formation, and regulation of the cytosolic c-ring, a dynamic component of the type III secretion injectisome. *PLoS Biol* 13(1):e1002039.
21. Diepold A, *et al.* (2017) A dynamic and adaptive network of cytosolic interactions governs protein export by the T3SS injectisome. *Nature communications* 8:15940.
22. Zhu S, *et al.* (2017) Molecular architecture of the sheathed polar flagellum in Vibrio alginolyticus. *Proceedings of the National Academy of Sciences of the United States of America*.
23. Schuster SC & Baeuerlein E (1992) Location of the basal disk and a ringlike cytoplasmic structure, two additional structures of the flagellar apparatus of Wolinella succinogenes. *Journal of bacteriology* 174(1):263-268.
24. Francis NR, Sosinsky GE, Thomas D, & DeRosier DJ (1994) Isolation, Characterization and Structure of Bacterial Flagellar Motors Containing the Switch Complex. *Journal of Molecular Biology* 235(4):1261-1270.
25. Kaniga K, Delor I, & Cornelis GR (1991) A wide-host-range suicide vector for improving reverse genetics in Gram-negative bacteria: inactivation of the blaA gene of Yersinia enterocolitica. *Gene* 109(1):137-141.
26. Diepold A, *et al.* (2010) Deciphering the assembly of the Yersinia type III secretion injectisome. *EMBO J* 29(11):1928-1940.
27. Ester M, Kriegel H-P, Sander J, & Xu X (1996) A density-based algorithm for discovering clusters a density-based algorithm for discovering clusters in large spatial databases with noise. in *Proceedings of the Second International Conference on Knowledge Discovery and Data Mining* (AAAI Press, Portland, Oregon), pp 226-231.
28. Zhang Y, Lara-Tejero M, Bewersdorf J, & Galan JE (2017) Visualization and characterization of individual type III protein secretion machines in live bacteria. *Proceedings of the National Academy of Sciences of the United States of America* 114(23):6098-6103.
29. Konopka MC, Shkel IA, Cayley S, Record MT, & Weisshaar JC (2006) Crowding and Confinement Effects on Protein Diffusion In Vivo. *Journal of bacteriology* 188(17):6115-6123.
30. Costantini LM, Fossati M, Francolini M, & Snapp EL (2012) Assessing the Tendency of Fluorescent Proteins to Oligomerize under Physiologic Conditions. *Traffic* 13(5):643-649.
31. McDowell MA, *et al.* (2016) Characterisation of Shigella Spa33 and Thermotoga FliM/N reveals a new model for C-ring assembly in T3SS. *Molecular microbiology* 99(4):749-766.
32. Elowitz MB, Surette MG, Wolf P-E, Stock JB, & Leibler S (1999) Protein Mobility in the Cytoplasm of Escherichia coli. *Journal of bacteriology* 181(1):197-203.
33. Kumar M, Mommer MS, & Sourjik V (2010) Mobility of cytoplasmic, membrane, and DNA-binding proteins in Escherichia coli. *Biophysical journal* 98(4):552-559.

34. Lew MD, von Diezmann ARS, & Moerner WE (2013) Easy-DHPSF open-source software for three-dimensional localization of single molecules with precision beyond the optical diffraction limit. *Protocol Exchange*:doi:10.1038/protex.2013.1026.

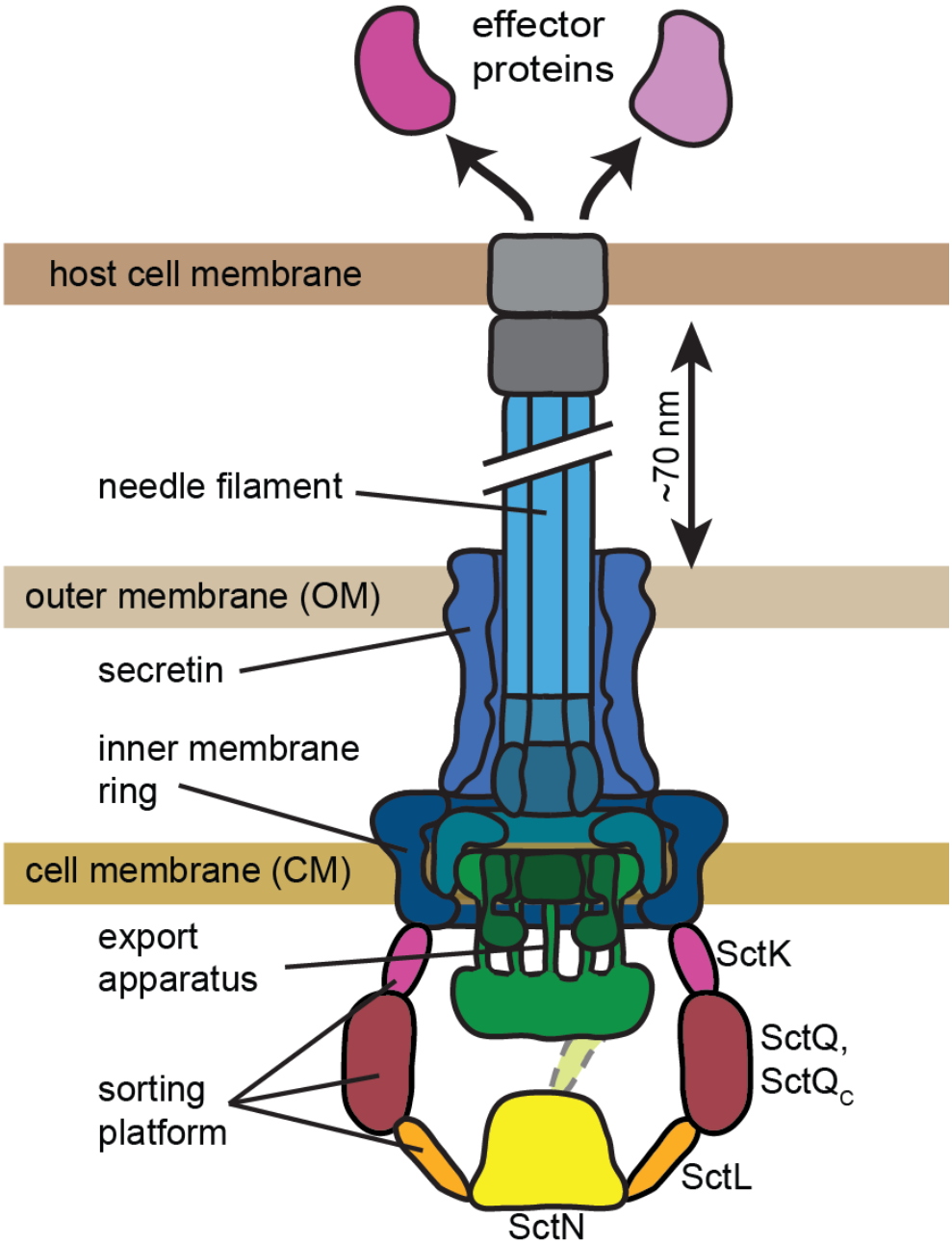

Fig. 1. The T3SS injectisome spans both the inner and outer bacterial membranes and features a long hollow needle that protrudes away from the cell surface. The injectisome is used to transport effector proteins from the bacterial cytosol into the cytosol of eukaryotic host cells. At the cytoplasmic interface of the fully assembled injectisome, three interacting proteins (SctL,Q,K) are essential for the function of the T3SS and together form a so-called sorting platform. SctL forms a cradle-like structure that connects the hexameric ATPase SctN to each of the six pods, which contain multiple SctQ (and likely SctQ$_C$) subunits (10). SctK is an auxiliary protein that resides between the SctQ pods and the inner membrane ring of the injectisome.

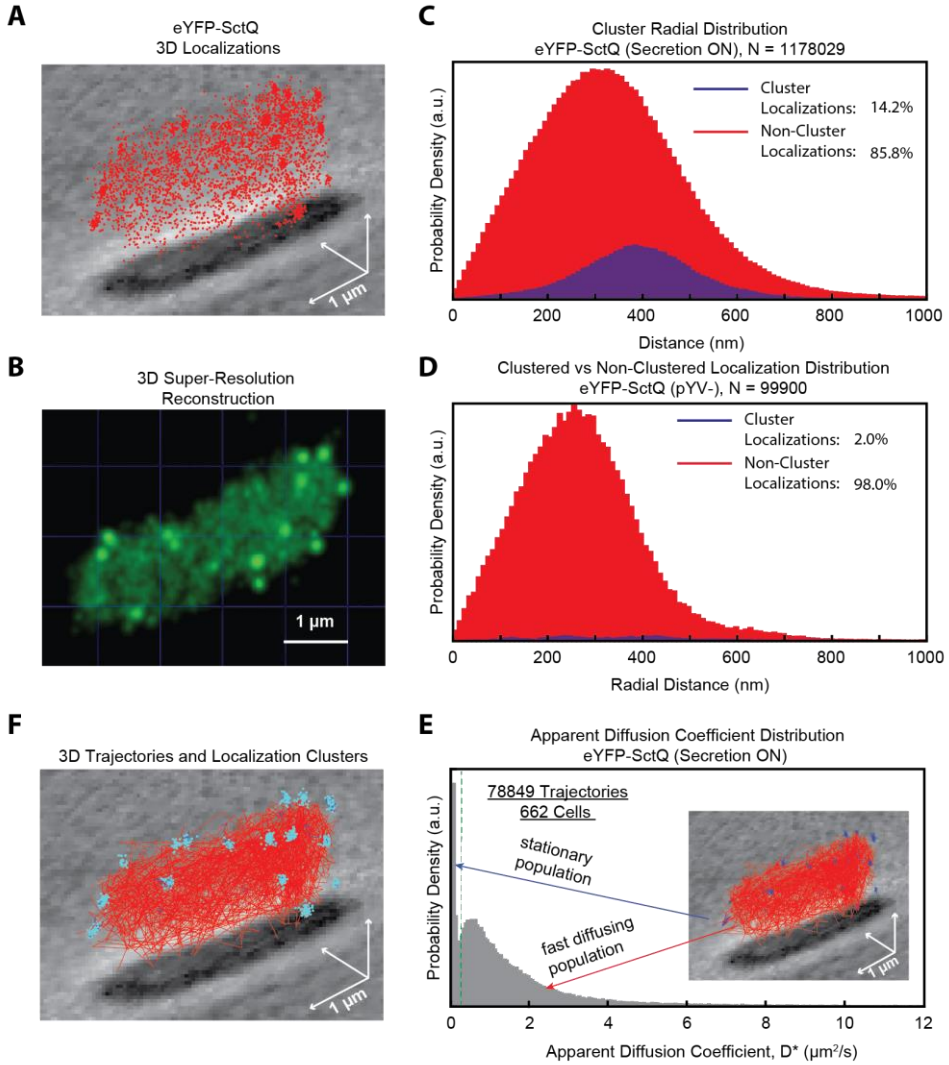

Fig. 2. Fluorescently labelled eYFP-SctQ localizes throughout the cytosol and forms distinct clustered foci near the membrane. (A) Scatter plot of 3D localizations of eYFP-SctQ in a representative wild-type *Y. enterocolitica* cell overlaid on a phase contrast image of the cell. (B) Super-resolution image of the data shown in (A). Each single-molecule localization was rendered as a Gaussian sphere of width σ equal to the average localization precision. Closely overlapping spheres generate high intensity in the reconstructed image. (C) Radial distribution of clusters as determined by the DBSCAN clustering algorithm (27). Clustered localizations are enriched near the cell membrane. (D) Radial distribution of clusters for eYFP-SctQ in the pYV- strain. Fewer clusters are present and do not preferentially localize near the cell membrane. (E) Probability density function of apparent diffusion coefficients for eYFP-SctQ. Two visually distinguishable populations emerge: a stationary ($D^* < 0.15$ µm^2/s) and a mobile population ($D^* > 0.15$ µm^2/s). (E inset) Stationary (blue) and diffusive (red) trajectories in a single *Yersinia* cell. (F) Clustered localizations (teal) overlaid on the trajectory plot. Across the population (N = 662 cells) 60% of all stationary trajectories co-localized with clustered regions (within 100 nm of the cluster center-of-mass).

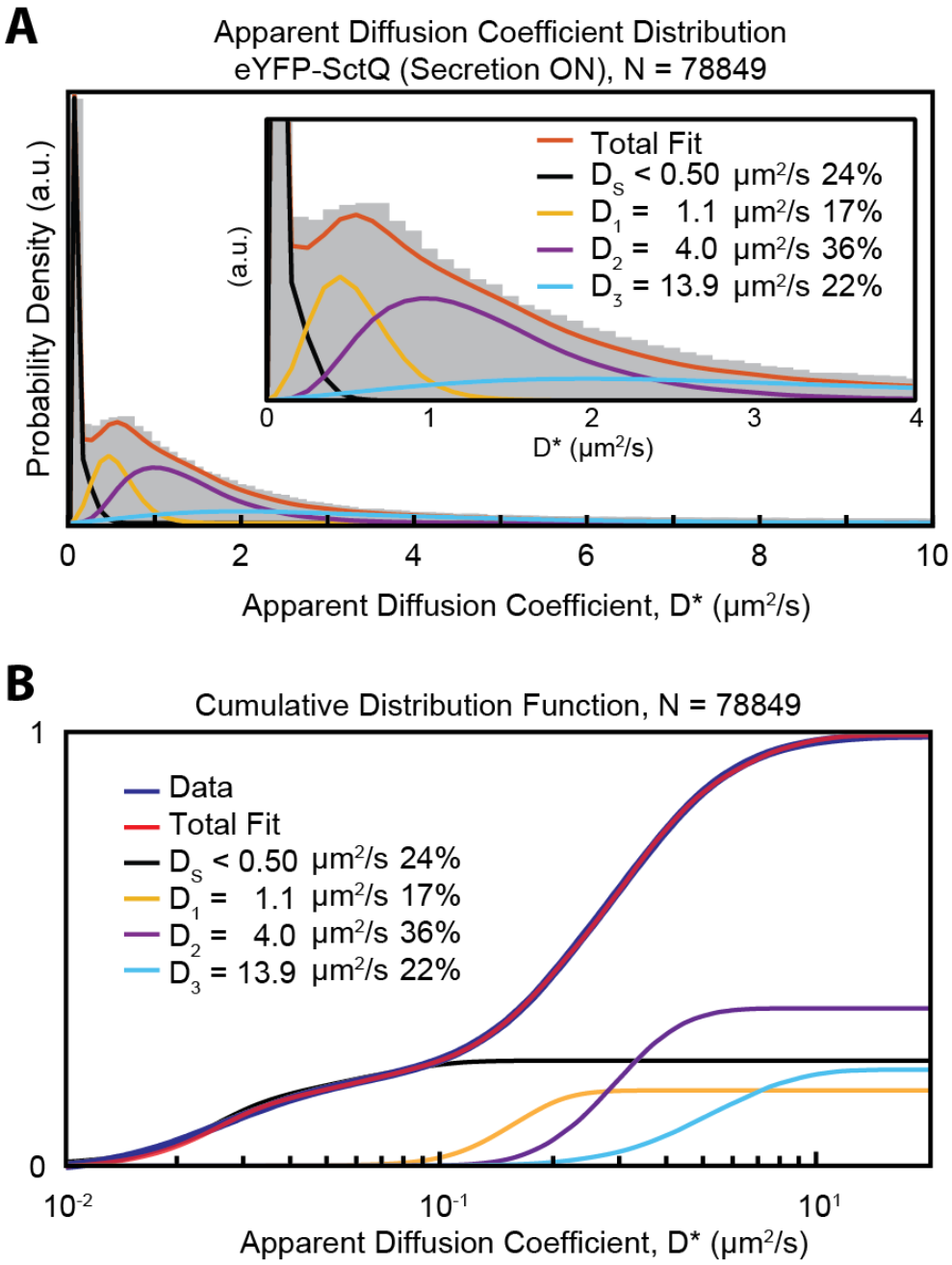

Fig. 3. Fit of the distribution of apparent diffusion coefficients for eYFP-SctQ. (A) Fitting the distribution of eYFP-SctQ apparent diffusion coefficients required at least three diffusive states ($D_{1\text{-}3}$) in addition to a stationary population (D_s). (B) The cumulative distribution function (CDF) of eYFP-SctQ apparent diffusion coefficients is fit using the indicated CDFs obtained by Monte-Carlo simulation of confined Brownian motion characterized by the indicated diffusion coefficients.

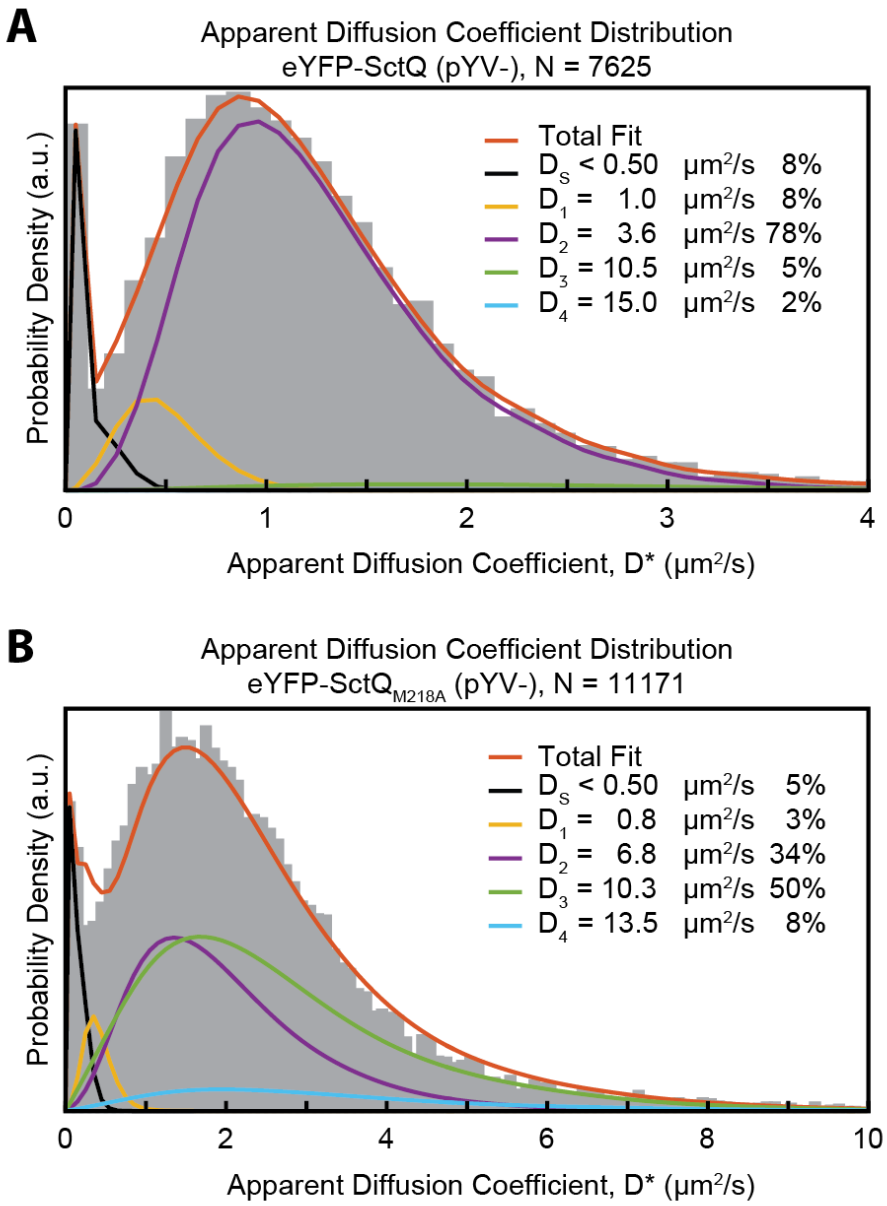

Fig. 4. Fit of the apparent diffusion coefficient distributions for eYFP-SctQ in the absence of other T3SS proteins. (A) Fitting of the eYFP-SctQ apparent diffusion coefficients distribution in the pYV- strain shows a dominant population at ~3.6 $\mu m^2/s$. (B) A mutation in the SctQ coding sequence that suppresses the expression of $SctQ_c$ eliminates the 3.6 $\mu m^2/s$ state and favors a faster diffusing state at 6.8 $\mu m^2/s$.

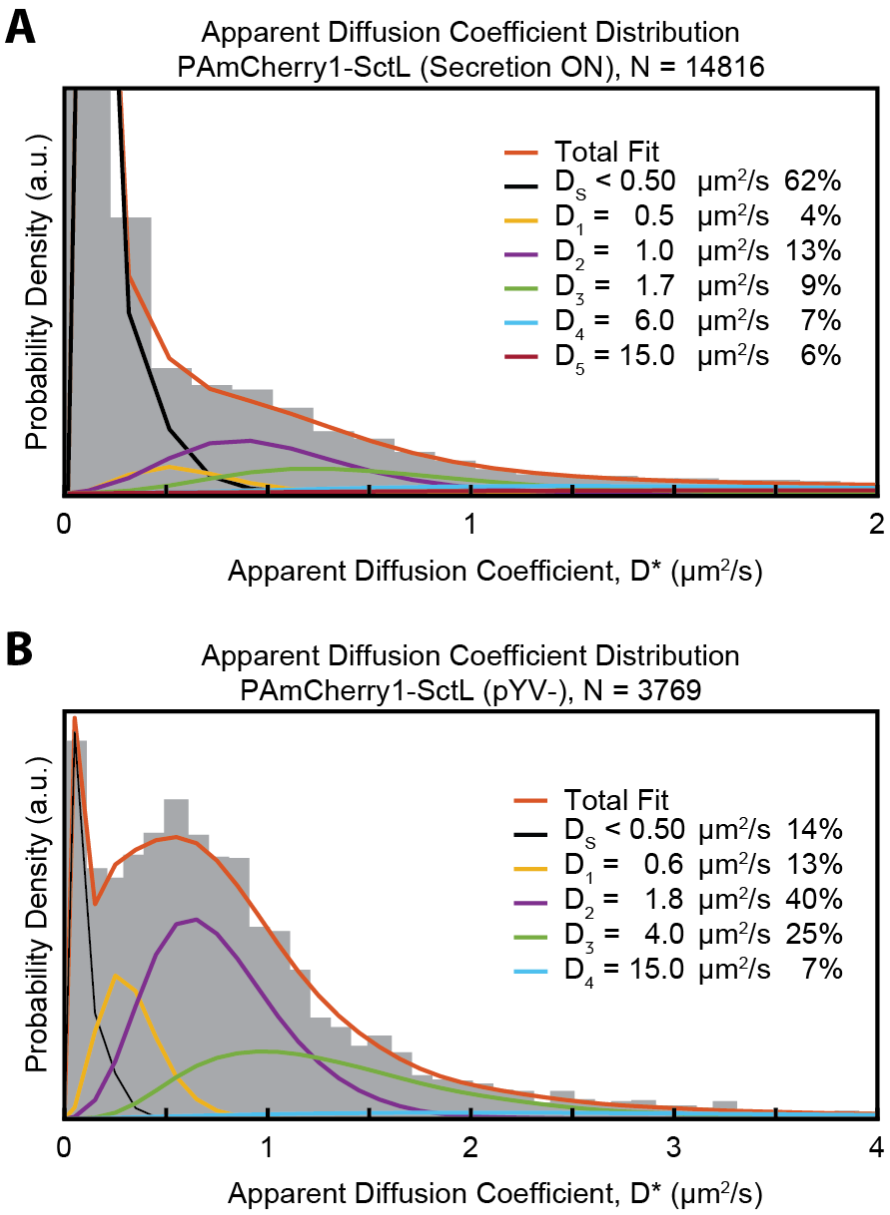

Fig. 5. Comparison of PAmCherry1-SctL in the wild-type vs the pYV- strain. (A) Fitting of the apparent diffusion coefficient distribution for PAmCherry1-SctL shows the majority of the population in a stationary state. (B) In the absence of other T3SS proteins the stationary state is depleted, and PAmCherry1-SctL favors faster diffusive states.

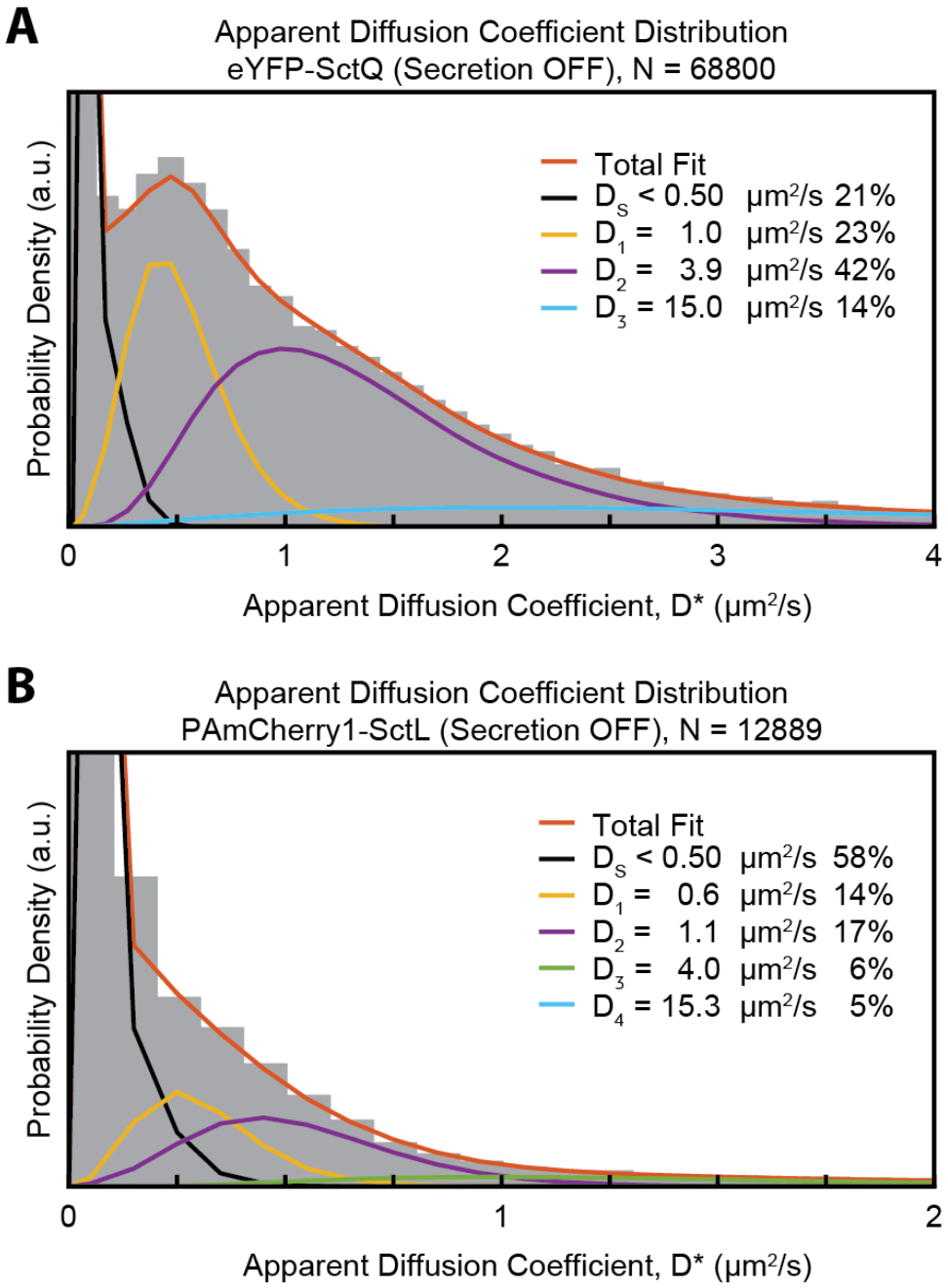

Fig. 6. Apparent diffusion coefficient distribution fits for eYFP-SctQ and PAmCherry1-SctL under secretion OFF conditions. (A) Fitting of secretion OFF conditions for eYFP-SctQ. While the individual diffusion coefficients remain the same as for secretion ON conditions, there is an overall population shift towards slower diffusing states. (B) Fitting of secretion OFF conditions for PAmCherry1-SctL. As is the case for eYFP-SctQ, there is a shift towards slower diffusing states for secretion OFF conditions.

Table 1. Fitted diffusion coefficients and relative population fractions.

eYFP-SctQ Secretion ON		**eYFP-SctQ Secretion OFF**		**eYFP-SctQ pYV-**		**eYFP-SctQ$_{M218A}$ pYV-**		**eYFP**	
(%)	*D* (μm^2/s)	%	*D* (μm^2/s)	%	*D* (μm^2/s)	%	*D* (μm^2/s)	%	*D* (μm^2/s)
24	<0.50	21	<0.50	8	<0.50	5	<0.50	3	<0.50
17	1.1	23	1.0	8	1.0	3	0.8	45	9.5
36	4.0	42	3.9	78	3.6	34	6.8	53	13.5
22	13.9	14	15.0	5	10.5	50	10.3		
				2	15.0	8	13.5		
PAmCherry1-SctL Secretion ON		**PAmCherry1-SctL Secretion OFF**		**PAmCherry1-SctL pYV-**				**PAmCherry1**	
%	*D* (μm^2/s)	%	*D* (μm^2/s)	%	*D* (μm^2/s)			%	*D* (μm^2/s)
62	<0.50	58	<0.50	14	<0.50			20	<0.50
4	0.5	14	0.6	13	0.6			13	2.7
13	1.0	17	1.1	40	1.8			68	15.3
9	1.7	6	4.0	25	4.0				
7	6.0	5	15.3	7	15.0				
6	15.0								